Accepted Manuscript

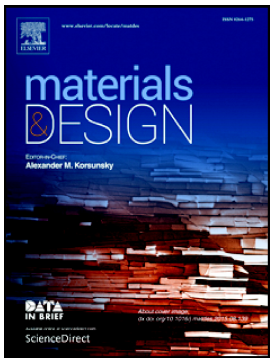

Crosslinked carbon nanofiber films with hierarchical pores as flexible electrodes for high performance supercapacitors

Jianping Ding, Hong-ping Zhang, Xiaodong Li, Youhong Tang, Guangcheng Yang

PII: S0264-1275(17)31134-6
DOI: https://doi.org/10.1016/j.matdes.2017.12.028
Reference: JMADE 3579

To appear in: *Materials & Design*

Received date: 29 October 2017
Revised date: 15 December 2017
Accepted date: 16 December 2017

Please cite this article as: Jianping Ding, Hong-ping Zhang, Xiaodong Li, Youhong Tang, Guangcheng Yang , Crosslinked carbon nanofiber films with hierarchical pores as flexible electrodes for high performance supercapacitors. The address for the corresponding author was captured as affiliation for all authors. Please check if appropriate. Jmade(2017), https://doi.org/10.1016/j.matdes.2017.12.028

Crosslinked carbon nanofiber films with hierarchical pores as flexible electrodes for high performance supercapacitors

Jianping Ding [a, b], Hong-ping Zhang [a, *], Xiaodong Li [b, *], Youhong Tang [c], Guangcheng Yang [b]

[a] Engineering Research Center of Biomass Materials, Ministry of Education, School of Materials Science and Engineering, Southwest University of Science and Technology, Mianyang, Sichuan 621010, China

[b] Institute of Chemical Materials, China Academy of Engineering Physics, Mianyang, Sichuan 621900, China

[c] Centre for NanoScale Science and Technology, College of Science and Engineering, Flinders University, South Australia 5042, Australia

[*] Corresponding authors. Tel: +86-816-6089009, Fax: +86-816-6089009, E-mail: zhp1006@126.com (H. P. Zhang); Tel: +86-816-2544426, Fax: +86-816-2544426, E-mail: lixdong2013@caep.cn (X. D. Li)

Abstract

Flexible, cross-linked carbon nanofibers (CNFs) film with hierarchical

micro-meso-macro-porous structure is prepared by carbonization of the elestrospun polyacrylonitrile (PAN)/NaN_3 composite nanofiber mats. The gas liberation of NaN_3 during the carbonization is responsible for the tuning of both specific surface area and the pore size distribution. In addition, the exothermal decomposition of NaN_3 at the heating stage of carbonization leads to the melting of the PAN/NaN_3 composite fibers, resulting in a cross-linked CNF structure. The CNF film with 5 wt.% NaN_3 carbonized at 900 ℃ (CNF-5-900) shows a high specific capacitance of 222.92 F g^{-1}, nearly twice as high as that of the CNF film without NaN_3 (CNF-0-900). It also shows an excellent capacitance retention ratio of 81.97 % of its initial capacitance from 0.5 A g^{-1} to 50 A g^{-1}, much superior to the value of 51.02 % for CNF-0-900. Moreover, it has an excellent cycling stability with cycling retention ratio achieves 94.5 % after 10,000 charge-discharge cycles. Coupled with its excellent mechanical stability (only 1.6 % conductivity loss after bending of CNF-5-900 film at curvature radii (r)=2.5×10^{-3} m for 10,000 cycles) and facile fabrication process, the flexible, cross-linked CNF films with hierarchical micro-meso-macro-porous structure is a potential electrode materials and/or backbone to support other active materials for various application, including the flexible energy storage and electrocatalytic.

Keywords: NaN_3, carbon nanofibers, flexible, hierarchical pores, supercapacitor electrode

1. Introduction

The ever-increasing energy demand of mankind and shortage of fossil fuel resources urgently require the innovation of the energy storage/conversion systems that are reliable, high efficiency, low-cost and environmentally friendly. Some electrochemical energy storage devices, like lithium-ion batteries (LiBs) and supercapacitors (SCs), have been developed in the past two or three decades, and have been broadly used in ours daily life [1]. Owing to their higher specific capacitance, superior power density and longer cycle life than other electrochemical energy storage devices, the SCs have attracted wide attention. In particular, the appearance of wearable electronics in recent years has opened new frontiers for high performance energy-storage devices that are lightweight, flexible, wearable, and bendable [1-4]. Flexible supercapacitors (SCs), a class of important energy-storage devices, are considered to be promising candidates for wearable electronics by virtue of their advantages of high power density, long cycle life, fast charging/discharging, and environment-friendliness compared with batteries [5-7]. To serve the needs of real applications, the capacitance of flexible SCs should meet current challenges that require high surface areas for large quantities of ion adsorption/desorption [8]. Various electrode materials with simultaneous high surface area and excellent flexibility have been used in flexible SCs, including graphene, carbon nanotubes (CNTs), conductive polymers, and so on [3, 9-13]. Conductive polymers have high specific capacitance (~2000 F g^{-1}) and good flexibility, but their cycling stability is too poor for practical SCs [14-16]. Graphene and CNT film with densely packaged films have been widely investigated due to their advantages of combining the merits of high cycling stability and mechanical stability [17-19]. However, the randomly stacked or bundled structure could significantly reduce the ion accessible specific surface area (SSA) and increase the contact resistance, resulting in a low specific capacitance.

3D carbon networks with continuously interconnected macro-porous structures have been developed to improve the capacitance of flexible SCs by virtue of their combined advantages of good flexibility, high conductivity, and large number of macrospores for efficient electrolyte penetration [1, 20-22]. Among the various 3D

networks, carbon nanofiber (CNF) networks are one of the most promising materials due to their easy access, low cost, and continuously interconnected networks for high conductivity [23, 24]. In carbon based SCs, the energy is stored in an electrochemical double layer (EDL) at the electrode/electrolyte interface via reversible charge adsorption/desorption, and thus the SSA is the key concern. As a result, recent work has focused on the preparation of CNF films with high SSA by adding a pore generator, using a mixture of different polymer precursors, tuning the carbonization conditions, and chemical activation such as KOH [25-28]. Even at the high SSA of 1160 $m^2 g^{-1}$, however, the capacitance of CNF based SCs is still low [28]. Previous work [25, 29-31] has demonstrated that adequate pore size is another key concern in determining the capacitance of SCs. It is reported that the charge storage in micropores (pores with diameters of 0.5 nm - 2 nm) increases with the decrease of pore size, but the poor accessibility of electrolyte ions in these pores limits the rate capability of the SCs [32, 33]. Mesopores (pores with diameter between 2 and 50 nm) have been demonstrated to contribute most to the capacitance in an EDL charge storage mechanism [34, 35]. The macropores (pores with diameter greater than 50 nm) could serve as an efficient pathway for electrolyte ions to access the inner micro- and mesopores, making them a prerequisite for high performance SCs. Thus, CNF with the synergistic advantages of high SSA and coexistence of hierarchical micro-meso-macro- pores should be developed using more preferred routes.

Due to its low cost and large-scale production capacity, electrospinning (ES) is one of the most widely used methods for producing porous CNFs [8, 20, 23, 26, 27, 36]. The morphology, surface area, and conductivity can be well controlled by tuning the precursors and the subsequent thermal treatment conditions [27, 37]. In particular, pore size can also be well controlled by ES. Li et al. [26] prepared a porous nitrogen-doping carbon nanofiber network by adjusting the content ratio of polyvinylpyrrolidone (PVP) to polyacrylonitrile (PAN) in PAN/PVP fibers, which generate a specific capacitance of 198 F g^{-1} at 1 A g^{-1} in 6M KOH. Lai et al. [38] reported that the decomposition of polymethyl methacrylate (PMMA) in electrospun PAN/PMMA composite fibers could generate pores, which could effectively increase

the SSA and pore volume of the fibers, and thus an increase of the specific capacitance by 38 % was obtained as compared to the neat PAN-derived CNFs. thereby enhancing capacitive performance. Wang et al. [25] prepared double-capillary carbon nanofibers with micropores in the inner capillary and mesopores in the outer capillary by coaxial electrospinning. The unique structure achieved better electrolyte accessibility and a shorter diffusion length for ions, showing an enhanced capacitance of 133 F g^{-1} and excellent rate performance. Lei et al. [39] produced the N-enriched CNF network by co-electrospinning of a PAN/PVP/SiO_2 blended solution, followed by pyrolysis and SiO_2 removal processes, resulting in a high pseudo-capacitance of 242 F g^{-1} and excellent cycling performance. These pioneering studies suggested that ES is a powerful technique for adjusting the pore structure and specific surface area of CNFs. However, in present methods, a hard/soft template and the concomitant post-treatment are required, limiting their appeal in real applications.

Based on the considerations described, an elegant strategy has been developed to tune the pore size distributions in ES CNFs using gas liberation of NaN_3 during the carbonization of the nanofibers. Due to the rapid decomposition of NaN_3, the pore size distribution within the nanofiber can be modified. The resultant CNF films show the coexistence of hierarchical micro-meso-macro- pores with the increase in SSA. Moreover, due to the exothermic decomposition reaction of NaN_3, the CNFs within the films melted together at their contact points, forming strong crosslinked CNF networks. Applied as self-supported flexible electrodes for SCs, the best sample, i.e., CNF film with 5 wt.% NaN_3 carbonized at 900 ^oC, defined as CNF-5-900 in this study, shows the highest specific capacitance of 222.92 F g^{-1}, nearly twice as high as that of CNF without NaN_3.

2. Experimental section

2.1 Preparation of CNF

To prepare the precursors for electrospinning, 0.5 g polyacrylonitrile (PAN, Sigma-Aldrich, US) was first dissolved in 4.5 g N, N-dimethylformamide (DMF, Kelong Chemical Reagent Plant, China) at room temperature under vigorous stirring

until it became clear. Then, NaN_3 (Chengdu Micxy Chemical Co. Ltd, China) was added into the solution and stirred for 2 h. To systematically investigate the effect of NaN_3 on pore distribution, NaN_3 with contents of 0, 3, 4, 5, and 6 wt. % to PAN was added, forming samples designated as CNF-0, CNF-3, CNF-4, CNF-5, and CNF-6, respectively. After stirring for 20 min, the precursors were obtained. During electrospinning, the applied voltage and the distance between needle and collector were fixed at 15 kV and 17 cm, respectively. Finally, nonwoven mats of PAN/NaN_3 composite nanofibers ~0.5 mm in thickness were obtained. Prior to carbonization, the nonwoven mats were dried at 60 ℃ for 6 h. For carbonization, the dried mats were stabilized at 260 ℃ for 3 h in air, and then heated to different temperatures (700 ℃, 800 ℃, 900 ℃, and 1000 ℃) in N_2 atmosphere at a heating rate of 5 ℃ min^{-1}. After holding each mat at the target temperature for 2 h, CNF mats with modified pore distribution were obtained.

2.2 Material characterization

The morphologies and structures of the samples were investigated by field emission scanning electron microscopy (FE-SEM, Ultra 55, Carl Zeiss, Germany) and transmission electron microscopy (TEM, Libra 200FE, Carl Zeiss, Germany). Raman spectroscopy was carried out on a Renishaw InVia Raman spectrometer equipped with a 514.5 nm laser. X-ray photoelectron spectra (XPS) were measured on a Thermo Scientific Escalab 250XI with an excitation source of Al Kα (1486.8 eV) radiation. The nitrogen adsorption-desorption isotherms of the samples were conducted on Autosrob-1 (Quantachrome instruments, US) by nitrogen adsorption at 77 K in the range of 1^{-6} to 1 atom. The SSA was determined from the N_2 adsorption/desorption isotherms using the Brunauer-Emmett-Teller (BET) equation.

2.3 Electrochemical measurements

All the electrochemical tests were performed on an electrochemical workstation (VMP3, BioLogic, France) at room temperature. Cyclic voltammogram (CV) curves, galvanostatic charge-discharge (GCD), and electrochemical impedance spectroscopy

(EIS) were measured in a standard three-electrode system with CNF films as the work electrode, a platinum plate as the counter electrode, and an Hg/HgO electrode as the reference electrode. The electrolyte was 6 M KOH aqueous solution. The EIS test was carried out at open circuit potential in the frequency range of 0.1 Hz~10^5 Hz at an alternating amplitude of 10 mV.

3. Results and discussion

The fabrication process of the CNF with modified pore structures is shown in Figure 1(a). The precursors containing NaN_3, PAN, and dimethylformamide were electrospun on a collection plate of aluminum foil to form a PAN/NaN_3 composite nanofiber mat. The NaN_3 is an ionic solid that occurs as a gas release reaction once it is detonated:

$$2NaN_3 \rightarrow 2Na + 3N_2$$

Because large quantities of gases are released during this reaction, NaN_3 is selected as the gas-forming component in many car airbag systems. Upon heating, a same reaction occurs when the salt is heated to approximately 300 ℃. Thus, gas liberation occurs in the PAN/NaN_3 composite nanofiber due to the thermal decomposition of NaN_3 in the carbonization process, which is expected to modify the pore structure of the CNFs. After carbonization of the nanofiber mat at different temperatures, CNFs films with modified pore structure could be achieved. Figure 1(b) shows images of the CNF-5 film, which has a good flexibility and can be bent into an 'S' shape without obvious fatigue in the structure, as shown in Figure 1(c). To further test the flexibility of the CNF film, the CNF-5 film was bent at different curvature radii (r). As shown in Figure 1(d), the conductivity of the CNF-5 film changes little upon bending at different r values from 8.5×10^{-3} m to 5×10^{-5} m. Moreover, the film retains 98.4% conductivity after bending for 10,000 cycles at r = 2.5×10^{-3} m, as shown in Figure 1(e), indicating excellent mechanical stability.

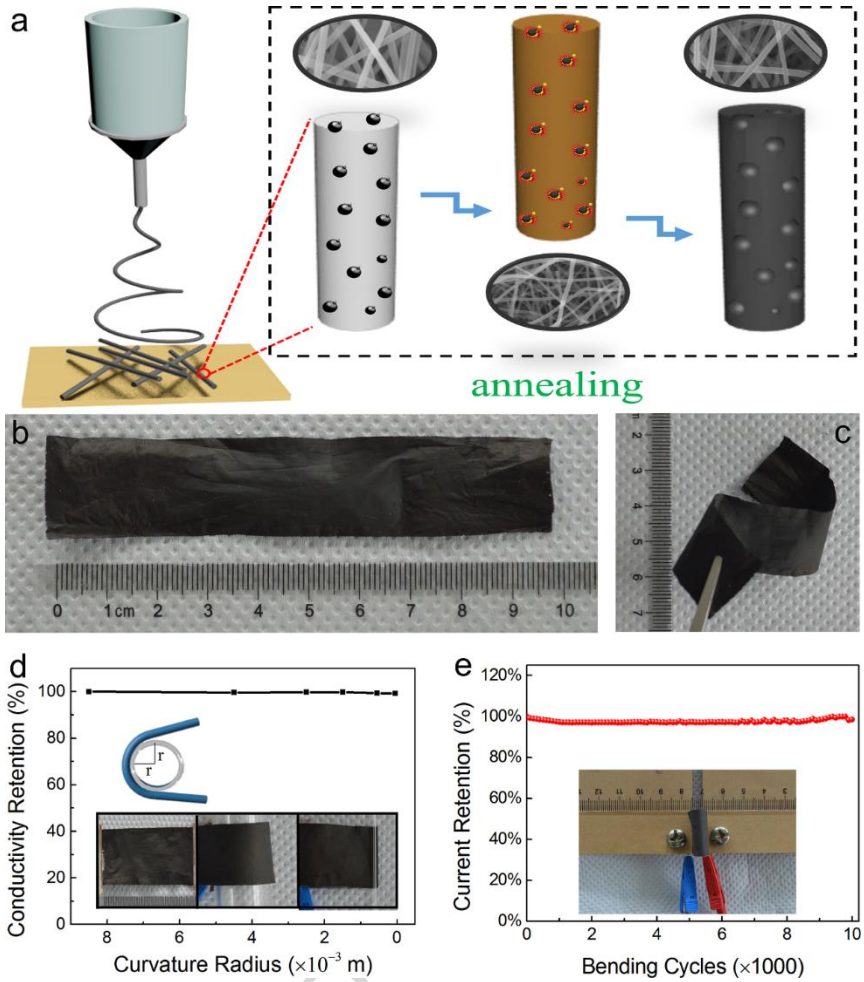

Figure 1. (a) Schematic illustration of the fabrication process of a flexible CNF electrode with modified pore structures. Images of the flexible CNF electrodes in (b) free and (c) bending states. (d) Conductivity retention of the CNF film at different curvature radii. Inset shows the images of the CNF film without bending and bending at different curvature radii, and (e) Current retention as a function of bending cycles for the CNF film.

Figure 2 shows SEM images of CNF prepared by carbonization of the electrospun PAN/NaN_3 composite nanofiber mats with different NaN_3 content within the precursors. The diameter of the CNF exhibits strong NaN_3 content dependence, decreasing from 228.08 nm for CNF-0 to 188.82 nm, 143.04 nm, 180.00 nm, and 167.93 nm for CNF-3, CNF-4, CNF-5, and CNF-6, respectively, as shown in Figure 2(a)-2(e). Moreover, the CNF mats prepared with NaN_3 show crosslinked carbon network structures. The higher the NaN_3 content, the stronger the cross-linking of

CNF. The formation of the crosslinked carbon network structure results from the exothermal decomposition reaction of NaN_3 during carbonization.

To investigate the structure of the CNF materials, Raman spectra were used to characterize the CNF film with different NaN_3 contents and the results are shown in Figure 2(f). All the samples show two characteristic peaks centered at 1353 cm^{-1} and 1580 cm^{-1}, corresponding to the carbon D-band and G-band, respectively. The D-band is associated with defects (defect sites or disordered sp^2 hybridized carbon atoms) in the graphite structure, whereas the G-band corresponds to in-plane vibrations of the graphitic structure [40]. The D-band to G-band intensity ratios (I_D/I_G) of the samples suggest the graphitization of the carbon materials. All the I_D/I_G values were greater than 1.00, indicating the amorphous structure of the CNF [41, 42]. TEM characterization further confirms the amorphous structure of the CNF, regardless of NaN_3 modifications, as shown in Figure 3.

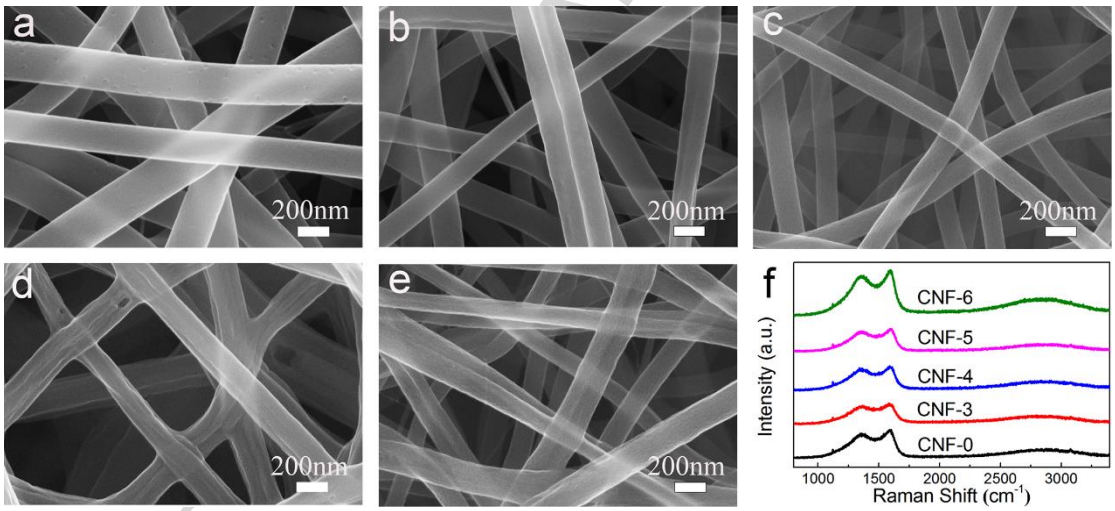

Figure 2. SEM images of (a) CNF-0, (b) CNF-3, (c) CNF-4, (d) CNF-5, (e) CNF-6, and (f) Raman spectra of different samples.

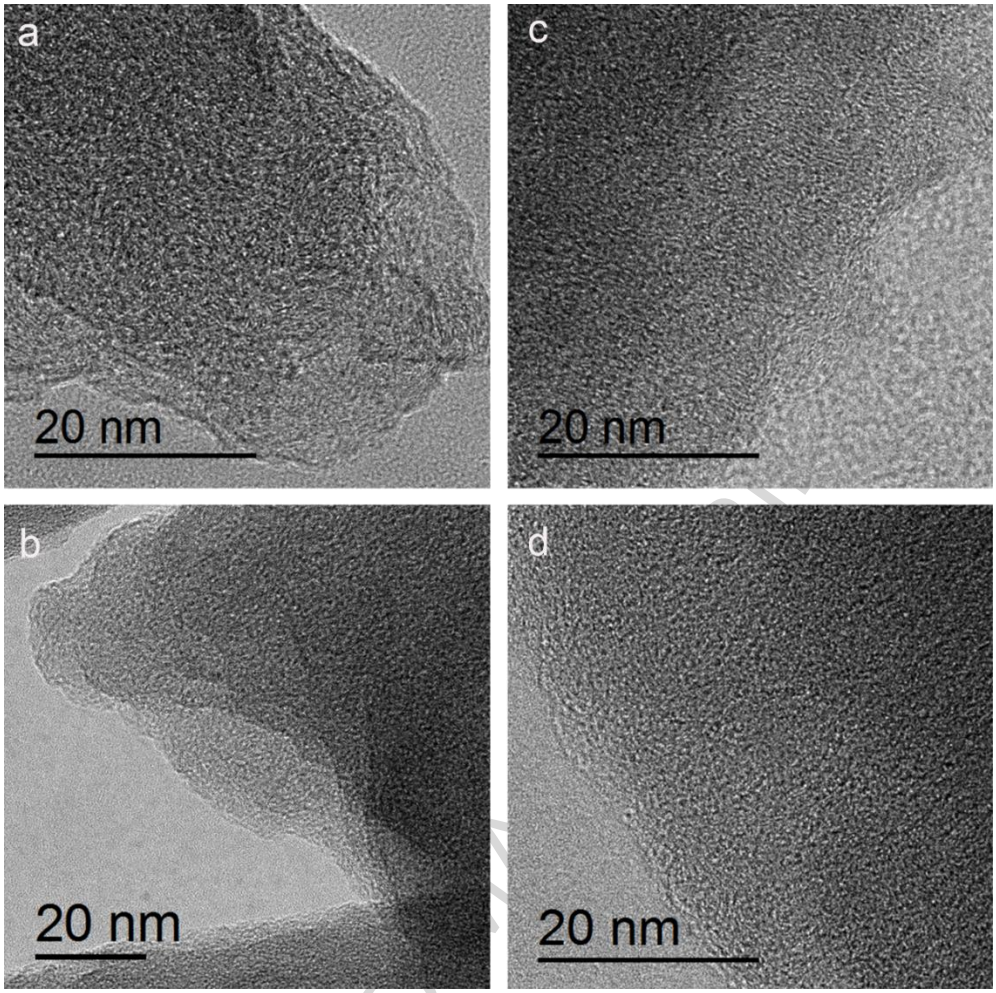

Figure 3. TEM images of (a) and (c) CNF-0 and (b) and (d) CNF-5 at different magnifications.

N_2 adsorption-desorption isotherms of the samples with and without NaN_3 modification were measured to investigate the porous structure of the CNF films (Figure 4), and the corresponding surface area and volume parameters are summarized in Table 1. As shown in Figure 4(a), all the isotherms can be identified as types I and IV for microporous and mesoporous structures according to the classification of the International Union of Pure and Applied Chemistry [27, 43-45]. As shown in Table 1, the CNF-5-900 possesses a BET surface area of 554.20 m^2 g^{-1} and a total pore volume (by using the Barrett-Joyner-Halenda method) of 0.38 cm^3 g^{-1}. Upon NaN_3 modification, the BET surface area and total pore volume are increased to 726.80 m^2 g^{-1} and 0.71 cm^3 g^{-1} respectively for CNF-5-900. The pore size distribution based on the density functional theory (DFT) method show two sharp peaks at 0.8 nm and 1.2 nm, and some wide peaks at 1.3 nm~5.0 nm, indicating the coexistence of

micropores and mesopores, a desired feature for SCs. It is noteworthy that the pore volume of CNF-0-900 mainly originates from micropores, the fraction of the mesopores is 16.28 %. While the fraction of the mesopores in CNF-5-900 are increased to 20.68 %, indicating the successful modification of the pore structure of the CNF by gas liberation of NaN_3 during the carbonization process. The surface area, the pore volume and the pore size distribution of the CNF with 5 wt. % NaN_3 exhibit strong temperature dependent behavior. The SSA and the total pore volume of the CNF with 5 wt.% NaN_3 increase with the temperature increased from 700 ℃ to 1000 ℃. The main source of the increase of the SSA and pore volume is the increase of the micropores and decrease of the mesopores as the temperature increases, as shown in Table 1. The CNF films with modified pore structure by gas liberation of NaN_3 is expected to greatly improve the capacitive performance of the CNF materials.

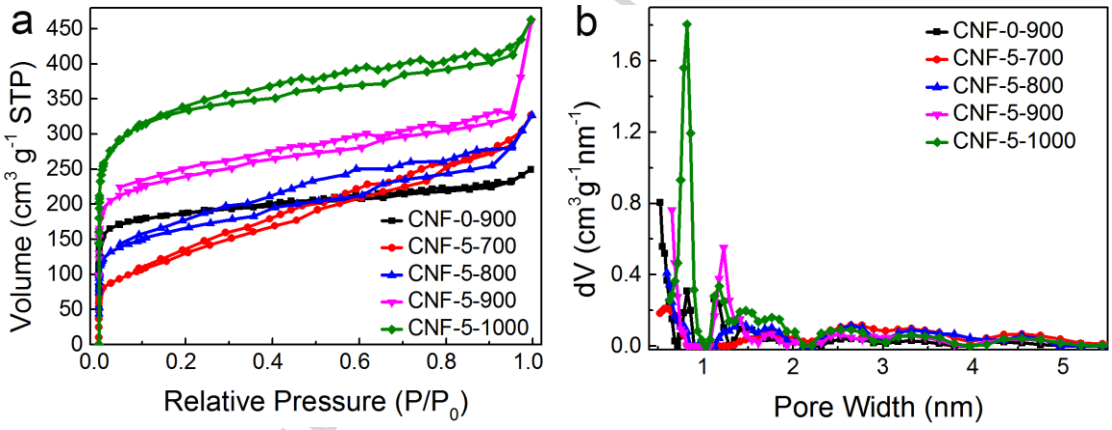

Figure 4. (a) N_2 adsorption/desorption isotherms and (b) pore size distribution of CNF-0-900 and CNF-5-900.

Table 1. Surface area and pore volume parameters of CNF-0-900, CNF-5-700, CNF-5-800, CNF-5-900 and CNF-5-1000.

Sample	S_{BET} (m^2 g^{-1})	V_{Total} (cc g^{-1})	S_{micro} (m^2 g^{-1})	S_{meso} (m^2 g^{-1})
CNF-0-900	554.20	0.3837	464.00	90.20
CNF-5-700	430.60	0.5024	61.02	415.3
CNF-5-800	551.40	0.5025	236.50	314.8
CNF-5-900	726.80	0.7089	576.50	150.3
CNF-5-1000	991.80	0.7121	825.10	166.7

The elemental composition and bonding configurations of the CNF-5 film carbonized at different temperatures were characterized by XPS, shown in Figure 5(a). Four peaks, corresponding to the binding energies of Na1s, C1s, N1s, and O1s, are observed. The C content of CNF-5 accumulates gradually from 79.35 % to 97.43 %, as the temperature increases from 700 ℃ to 1000 ℃, while the nitrogen and oxygen contents decrease from 9.66 % and 8.56 % to 0.59 % and 1.99 % respectively. The Na element in CNF-5-700 and CNF-5-800 is the residue of NaN_3, which diminishes with increase in temperature and is absent when the temperature is higher than 900 ℃. The increase in C content and reduction in Na and O content is beneficial to the formation of graphitic C-C bonds and the promotion of conductivity of the CNF, resulting in the improvement of the electrochemical performance of CNF films [26, 27, 46]. The high-resolution N1s spectra provide precise identification of the N configuration and N content in CNF. All the N1s spectra can be deconvoluted into three individual peaks centered at 398, 400, and 401 eV, corresponding to pyridinic N (N-6), pyrrolic N (N-5), and graphitic N (N-Q), respectively [47], as shown in Figure 5(b)-4(f). The N content of CNF shows strong temperature dependence, decreasing from 9.66% in CNF-5-700 to 6.96%, 2.17%, and 0.59% in CNF-5-800, CNF-5-900, and CNF-5-1000 respectively, consistent with previous reports [10, 48].

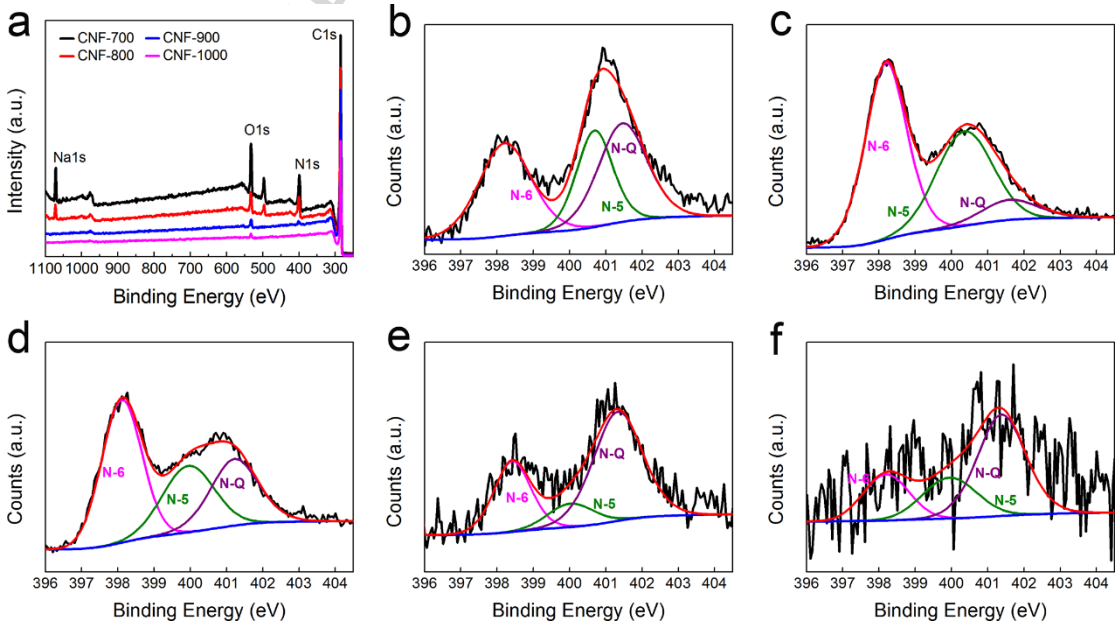

Figure 5. (a) XPS survey spectra of CNF-700, CNF-800, CNF-900, and CNF-1000;

high-resolution XPS N1s spectra of (b) CNF-0-900, (c) CNF-5-700, (d) CNF-5-800, (e) CNF-5-900, and (f) CNF-5-1000. The black curves in 5(b)-5(f) are the experimental results that can be fitted to three synthetic peaks and the red curve is the summation of the synthetic peaks.

To evaluate the electrochemical performance of the NaN_3 modified CNF films, CV and GCD measurements were carried out in a three-electrode system. The NaN_3 content is an important parameter that influences the capacitive performance of the CNF films, as illustrated in Figure 6(a). The CNF film without NaN_3 modification shows a specific capacitance of 102.96 F g^{-1} (calculated from the CV curves), a finding that is comparable to the reported values of CNF based SCs [49, 50]. As the content of NaN_3 increases, the specific capacitance of the CNF film increases sharply to 173.14 and 166.24 F g^{-1} for CNF-3 and CNF-4 respectively, and reaches a maximum value of 218.32 F g^{-1} for CNF-5, as shown in Figure 6(a).

Carbonization temperature is another key factor that determines the capacitive performance of the CNF film based SCs. As shown in Figure 6(b), both CNF-0 and CNF-5 show a carbonization temperature dependent behavior. The specific capacitance of CNF-0 increases slightly from 92.21 F g^{-1} to 133.56 F g^{-1} as the temperature increases from 700 ℃ to 1000 ℃, whereas the specific capacitance of CNF-5 shows a stronger temperature dependence, increasing sharply from 62.81 F g^{-1} at 700 ℃ to a maximum value of 222.92 F g^{-1} at 900 ℃, followed by a sharp decrease with further increase in the temperature to 1000 ℃. And more data of all samples were listed in Table S1.

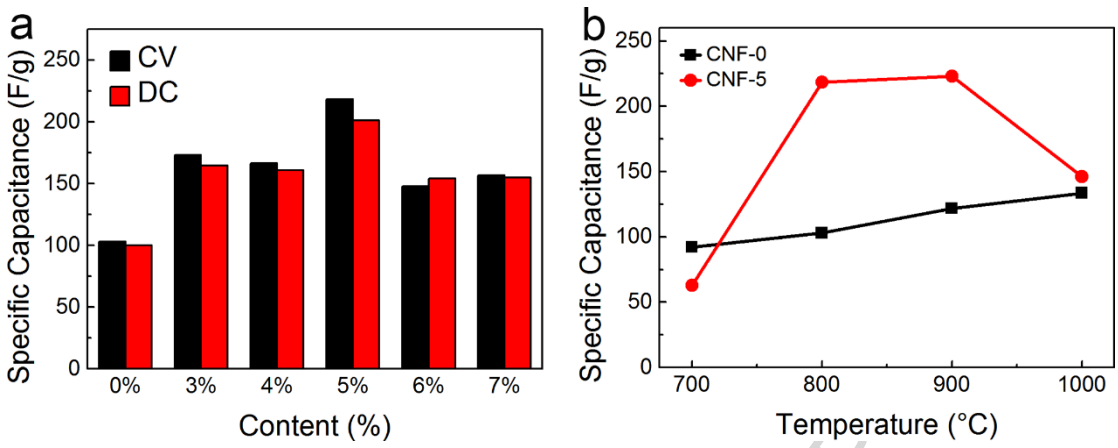

Figure 6. Electrochemical performance of porous CNF electrodes in a three-electrode system using 6 M KOH electrolyte between -0.8 eV and 0.0 eV. (a) Mass specific capacitance contrast of different CNF-x electrodes at 20 mV/s (black bar) and 1 A/g (red bar) and (b) the specific capacitance of CNF-0 and CNF-5 ranging from 700 ℃ to 1000 ℃.

The CNF films prepared with optimized parameters (5 wt% NaN_3 carbonized at 900 ^oC) were further characterized by CV experiments in a voltage window of -0.8 V-0 V vs. Hg/HgO at different scan rates ranging from 2 to 100 mV s^{-1}. The quasi-rectangular shapes of the CV curves indicate the pure EDLC behavior of CNF-5-900, as shown in Figure 7(a). The shapes of the CV curves at high scan rates are similar to those at low scan rates, and the shapes show no obvious distortion, even at the high scan rate of 100 mV s^{-1}. Figure 7(b) shows the GCD behavior of CNF-5-900 between 0 and -0.8 V at different current densities. The GCD curves are close to triangular in shape, even at the high current density of 100 A g^{-1}, consistent with the results of the CV curves. Both CV and GCD results confirm the formation of an efficient EDLC and efficient ionic and electronic transport within the CNF-5-900 electrodes, features that are essential to obtaining fast charge/discharge rates. We also tested the rate performance of the CNF film based SCs, that is a crucial factor for their practical application as energy-storage devices. As shown in Figure 7(c), the capacitance retention ratio (the ratio of the capacitance at 50 A g^{-1} as compared to the value at 0.5 A g^{-1}) of CNF-5-900 is as high as 81.97%, higher than that of CNF-0-900

(51.02%), indicating that the CNF-5-900 film with modified pore structures and cross-linked networks facilitates the formation of EDLC and the enhancement of ionic and electronic transport within the CNF-5-900 electrodes. EIS was conducted to elucidate the role of NaN_3 modification on the super-capacitive performance of the CNF [12, 25]. As shown in Figure 7(d), Nyquist plots of CNF-0-900 and CNF-5-900 based SCs show linear behavior and high slopes (close to 90^o) in the low-frequency region, revealing ideal capacitive behavior of the electrodes. It is noteworthy that CNF-5-900 shows a smaller semicircle at high-frequency regions compared to that of CNF-0-900, indicating lower mass transfer resistance and better ion propagation behavior in CNF-5-900 than in CNF-0-900. Moreover, CNF-5-900 shows a lower equivalent series resistance (ESR) of 6.28 ohm compared to 7.14 ohm for CNF-0-900, suggesting lower conductivity of CNF-5-900. The EIS results reveal that the modified pore structures and cross-linked matrix of CNF-5-900 result in lower electron resistance and better ion diffusion behavior as compared with that of CNF-0-900, which increase not only the specific capacitance but also the rate performance of the CNF based SC. Additionally, the CNF-5-900 SC exhibits excellent cycling stability, with 94.5% of its original value after 10,000 cycles of GCD measurements, as shown in Figure 7(e).

The comparison of major characteristics of the present results with literature on carbon-based SCs is listed in Table 2. The maximum specific capacitance of the present CNF-5-900 is 228.75 F g^{-1} at 1 A/g, among one of the highest values achieved by carbon-based SCs. A capacitance retention ratio of 81.97% (50 A g^{-1} as compared to the value at 0.5 A g^{-1}) is higher than most of the values previously reported for carbon-based electrodes, particularly as the previous studies were carried out at significantly lower current densities. Moreover, few reported materials are flexible to serve the needs of wearable electronics, particularly the one with simultaneously high capacitive performance, facile preparation process and excellent flexibility.

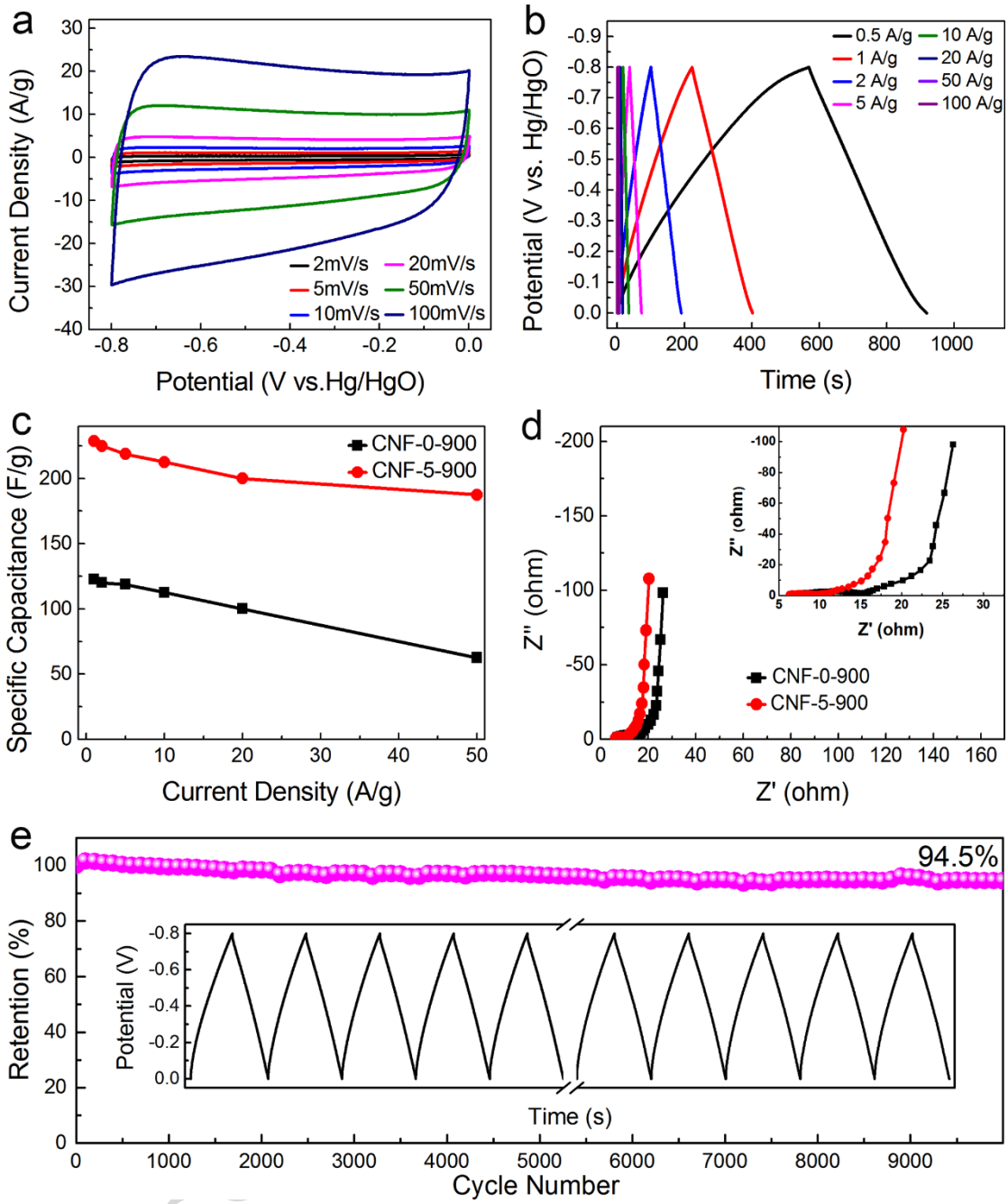

Figure 7. (a) CV curves of the CNF-5-900 electrode at scan rates ranging from 2 mV/s to 100 mV/s. (b) Galvanostatic charge/discharge curves of the CNF-5-900 electrode at current densities ranging from 0.5A/g to 100 A/g. (c) Specific capacitance of CNF-0-900 and CNF-5-900 at different densities. (d) Nyquist plots showing the imaginary part vs. the real part of the impedance of CNF-0-900 and CNF-5-900 and (e) Cycle life of CNF-5-900 after 10000 cycles with insert showing the first 5 and the last 5 cycles.

Table 2. Comparison of the electrochemical performance of different carbon electrode materials as supercapabitors from various precursors

Precursors	Sample	Flex	S_{BET} (m^2 g^{-1})	C_{sp} (F g^{-1})	Rate capability	Ref.
Biochar/PAN	CNF	Yes	30.12	37.6 F g^{-1} at 0.5 A/g	/	[51]
PAN/SiO_2	Hollow Carbon Capsule	No	718.0	206.0 F g^{-1} at 1 A/g	61.50 % at 10 A/g	[52]
PAN/PVP	CNF	No	452.5	198.0 F g^{-1} at 1 A/g	54.80 % at 40 A/g	[26]
PAN/PMMA	CNF	No	812.6	185.0 F g^{-1} at 5 mV/s	< 60.00 % at 300 mV/s	[53]
Cellulose	Porous carbon aerogel	No	646.0	195.0 F g^{-1} at 0.1 A/g	83.00 % at 20 A/g	[49]
PAN/POSS	CNF	No	335.38	257.7 F g^{-1} at 5 mV/s	45.40 % at 100 mV/s	[54]
PVP@TEOS/ lignin	CNF	Yes	870	245.0 F g^{-1} at 0.5 A/g	68.00 % at 30 A/g	[25]
PVA-GO/ PEDOT	CNF	No	/	224.27 F g^{-1} at 1 A/g	/	[55]
Chitosan/ Cellulose	Carbon cryogel	No	285.2	173.1 F g^{-1} at 1 A/g	/	[56]
PAN/NaN_3	CNF	Yes	726.8	228.75 F g^{-1} at 1 A/g	81.97 % at 50 A/g	This work

4. Conclusions

In this study, flexible CNF films with modified pore structures and cross-linked matrices were prepared by carbonization of electrospun PAN/NaN_3 composite nanofiber mats. NaN_3 not only modified the pore structure of the CNF fibers but also resulted in welding of the nanofibers, reducing both electron and ion diffusion impedance within the CNF based SCs. These advances offer a remarkable electrochemical performance. The greatest specific capacitance of the CNF film with 5% NaN_3 (CNF-5-900) reached 222.92 F g^{-1}, much higher than that of CNF film without added NaN_3 (CNF-0-900, 121.89 F g^{-1}). Furthermore, CNF-5-900 had a high rate capability of 81.97%, superior to the value of 51.02% for CNF-0-900. These intriguing features make CNF-5-900 a promising freestanding electrode for flexible SCs.

Acknowledgements

This research was supported by the National Natural Science Foundation of China (11272292, 11372288, 11502242, 51402269 and 11502247), the Development Foundation of CAEP (2014B302041), the Applied Basic Research Program of Sichuan Province (2015JY0229), and the Open Project of State Key Laboratory Cultivation Base for Nonmetal Composites and Functional Materials (14zxfk08).

References

[1] W. Liu, M.S. Song, B. Kong, Y. Cui, Flexible and Stretchable Energy Storage: Recent Advances and Future Perspectives, Adv. Mater. 29 (2017) 1603436.

[2] J. Cherusseri, R. Sharma, K.K. Kar, Helically coiled carbon nanotube electrodes for flexible supercapacitors, Carbon 105 (2016) 113-125.

[3] W. Zeng, L. Shu, Q. Li, S. Chen, F. Wang, X.M. Tao, Fiber-Based Wearable Electronics: A Review of Materials, Fabrication, Devices, and Applications, Adv. Mater. 26 (2014) 5310-5336.

[4] X. Li, X. Li, J. Cheng, D. Yuan, W. Ni, Q. Guan, L. Gao, B. Wang, Fiber-shaped solid-state supercapacitors based on molybdenum disulfide nanosheets for a self-powered photodetecting system, Nano Energy 21 (2016) 228-237.

[5] B. Yao, J. Zhang, T. Kou, Y. Song, T. Liu, Y. Li, Paper-Based Electrodes for Flexible Energy Storage Devices, Adv. Sci. 4 (2017) 1700107.

[6] J. Xu, F. Xu, M. Qian, F. Xu, Z. Hong, F. Huang, Conductive Carbon Nitride for Excellent Energy Storage, Adv. Mater. 29 (2017) 1701674.

[7] S. Li, Y.F. Dong, D.D. Wang, W. Chen, L. Huang, C.W. Shi, L.Q. Mai, Hierarchical nanowires for high-performance electrochemical energy storage, Front. Phys. 9 (2014) 303-322.

[8] D. Go, P. Lott, J. Stollenwerk, H. Thomas, M. Moller, A.J. Kuehne, Laser Carbonization of PAN-Nanofiber Mats with Enhanced Surface Area and Porosity, ACS Appl. Mater. Interfaces 4 (2016) 28412-28417.

[9] Y.K. Kim, S.I. Cha, S.H. Hong, Y.J. Jeong, A new hybrid architecture consisting of highly mesoporous CNT/carbon nanofibers from starch, J. Mater. Chem. 22 (2012) 20554-20560.

[10] H. Liu, Y. Zhang, R. Li, X. Sun, S. Désilets, H. Abou Rachid, M. Jaidann, L.S. Lussier, Structural and morphological control of aligned nitrogen-doped carbon nanotubes, Carbon 48 (2010) 1498-1507.

[11] T. Chen, L. Dai, Carbon nanomaterials for high-performance supercapacitors, Mater. Today 16 (2013) 272-280.

[12] R.A. Dar, G.A. Naikoo, P.K. Kalambate, L. Giri, F. Khan, S.P. Karna, A.K. Srivastava, Enhancement of the energy storage properties of supercapacitors using graphene nanosheets dispersed with macro-structured porous copper oxide, Electrochim. Acta 163 (2015) 196-203.

[13] J. Yan, T. Wei, Z. Fan, W. Qian, M. Zhang, X. Shen, F. Wei, Preparation of graphene nanosheet/carbon nanotube/polyaniline composite as electrode material for supercapacitors, J. Power Sources 195 (2010) 3041-3045.

[14] K. Halab Shaeli Iessa, Y. Zhang, G. Zhang, F. Xiao, S. Wang, Conductive porous sponge-like ionic liquid-graphene assembly decorated with nanosized polyaniline as active electrode material for supercapacitor, J. Power Sources 302 (2016) 92-97.

[15] J. Pedrós, A. Boscá, J. Martínez, S. Ruiz Gómez, L. Pérez, V. Barranco, F. Calle,

Polyaniline nanofiber sponge filled graphene foam as high gravimetric and volumetric capacitance electrode, J. Power Sources 317 (2016) 35-42.

[16] L. Liu, Z. Niu, L. Zhang, W. Zhou, X. Chen, S. Xie, Nanostructured Graphene Composite Papers for Highly Flexible and Foldable Supercapacitors, Adv. Mater. 26 (2014) 4855-4862.

[17] F. Su, X. Lv, M. Miao, High-Performance Two-Ply Yarn Supercapacitors Based on Carbon Nanotube Yarns Dotted with Co_3O_4 and NiO Nanoparticles, Small 11 (2015) 854-861.

[18] J. Ren, W. Bai, G. Guan, Y. Zhang, H. Peng, Flexible and Weaveable Capacitor Wire Based on a Carbon Nanocomposite Fiber, Adv. Mater. 25 (2013) 5965-5970.

[19] Z. Xu, C. Gao, Graphene chiral liquid crystals and macroscopic assembled fibres, Nat. Commun. 2 (2011) 571-580.

[20] Y. Cheng, L. Huang, X. Xiao, B. Yao, L. Yuan, T. Li, Z. Hu, B. Wang, J. Wan, J. Zhou, Flexible and cross-linked N-doped carbon nanofiber network for high performance freestanding supercapacitor electrode, Nano Energy 15 (2015) 66-74.

[21] G. Ren, S. Li, Z.-X. Fan, M.N.F. Hoque, Z. Fan, Ultrahigh-rate supercapacitors with large capacitance based on edge oriented graphene coated carbonized cellulous paper as flexible freestanding electrodes, J. Power Sources 325 (2016) 152-160.

[22] Z. Zhang, Y. Zhang, X. Mu, J. Du, H. Wang, B. Huang, J. Zhou, X. Pan, E. Xie, The carbonization temperature effect on the electrochemical performance of nitrogen-doped carbon monoliths, Electrochim. Acta 242 (2017) 100-106.

[23] L. Li, S. Peng, J.K.Y. Lee, D. Ji, M. Srinivasan, S. Ramakrishna, Electrospun hollow nanofibers for advanced secondary batteries, Nano Energy 39 (2017) 111-139.

[24] M. Xu, M. Wang, H. Xu, H. Xue, H. Pang, Electrospun-Technology-Derived High-Performance Electrochemical Energy Storage Devices, Asian. J. Chem. 11 (2016) 2967-2995.

[25] J. Wang, J. Tang, Y. Xu, B. Ding, Z. Chang, Y. Wang, X. Hao, H. Dou, J.H. Kim, X. Zhang, Y. Yamauchi, Interface miscibility induced double-capillary carbon

nanofibers for flexible electric double layer capacitors, Nano Energy 28 (2016) 232-240.

[26] X. Li, Y. Zhao, Y. Bai, X. Zhao, R. Wang, Y. Huang, Q. Liang, Z. Huang, A Non-Woven Network of Porous Nitrogen-doping Carbon Nanofibers as a Binder-free Electrode for Supercapacitors, Electrochim. Acta 230 (2017) 445-453.

[27] Y. Bai, Z.H. Huang, F. Kang, Electrospun preparation of microporous carbon ultrafine fibers with tuned diameter, pore structure and hydrophobicity from phenolic resin, Carbon 66 (2014) 705-712.

[28] H.M. Lee, H.G. Kim, S.J. Kang, S.J. Park, K.H. An, B.J. Kim, Effects of pore structures on electrochemical behaviors of polyacrylonitrile (PAN)-based activated carbon nanofibers, J. Ind. Eng. Chem. 21 (2015) 736-740.

[29] C. Burda, X. Chen, R. Narayanan, M.A. El Sayed, Chemistry and Properties of Nanocrystals of Different Shapes, Chem. Rev. 105 (2005) 1025-1102.

[30] B.J. Melde, B.J. Johnson, Mesoporous materials in sensing: morphology and functionality at the meso-interface, Anal. Bioanal. Chem. 398 (2010) 1565-1573.

[31] W. Dewei, W. Qihua, W. Tingmei, Controlled synthesis of mesoporous hematite nanostructures and their application as electrochemical capacitor electrodes, Nanotechnology 22 (2011) 135604-135616.

[32] J. Gamby, P.L. Taberna, P. Simon, J.F. Fauvarque, M. Chesneau, Studies and characterisations of various activated carbons used for carbon/carbon supercapacitors, J. Power Sources 101 (2001) 109-116.

[33] J. Chmiola, G. Yushin, Y. Gogotsi, C. Portet, P. Simon, P.L. Taberna, Anomalous Increase in Carbon Capacitance at Pore Sizes Less Than 1 Nanometer, Science 313 (2006) 1760-1763.

[34] R.W.P. S. T. Mayer, J. L. Kaschmitter, The Aerocapacitor: An Electrochemical Double-Layer Energy-Storage Device, J. Electrochem. Soc. 140 (1993) 446-451.

[35] B. Kastening, W. Schiel, M. Henschel, Electrochemical polarization of activated carbon and graphite powder suspensions, J. Electroanal. Chem. 191 (1985) 311-328.

[36] M.M. Jesse T. McCann, and Younan Xia, Highly Porous Fibers by

Electrospinning into a Cryogenic Liquid, J. Am. Chem. Soc. 128 (2006) 1436-1437.

[37] Q. Dong, G. Wang, H. Hu, J. Yang, B. Qian, Z. Ling, J. Qiu, Ultrasound-assisted preparation of electrospun carbon nanofiber/graphene composite electrode for supercapacitors, J. Power Sources 243 (2013) 350-353.

[38] C.C. Lai, C.T. Lo, Preparation of Nanostructural Carbon Nanofibers and Their Electrochemical Performance for Supercapacitors, Electrochim. Acta 183 (2015) 85-93.

[39] L. Fan, L. Yang, X. Ni, J. Han, R. Guo, C. Zhang, Nitrogen-enriched meso-macroporous carbon fiber network as a binder-free flexible electrode for supercapacitors, Carbon 107 (2016) 629-637.

[40] M. Kruk, K.M. Kohlhaas, B. Dufour, E.B. Celer, M. Jaroniec, K. Matyjaszewski, R.S. Ruoff, T. Kowalewski, Partially graphitic, high-surface-area mesoporous carbons from polyacrylonitrile templated by ordered and disordered mesoporous silicas, Micropor. Mesopor. Mat 102 (2007) 178-187.

[41] C. Zhang, R. Kong, X. Wang, Y. Xu, F. Wang, W. Ren, Y. Wang, F. Su, J.X. Jiang, Porous carbons derived from hypercrosslinked porous polymers for gas adsorption and energy storage, Carbon 114 (2017) 608-618.

[42] S.H. Yoo, H.I. Joh, S. Lee, Synthesis of porous carbon nanofiber with bamboo-like carbon nanofiber branches by one-step carbonization process, Appl. Surf. Sci. 402 (2017) 456-462.

[43] C. Kim, K.S. Yang, W.J. Lee, The Use of Carbon Nanofiber Electrodes Prepared by Electrospinning for Electrochemical Supercapacitors, Electrochem. Solid-State Lett. 7 (2004) 397-399.

[44] C.H. Kim, J.-H. Wee, Y.A. Kim, K.S. Yang, C.-M. Yang, Tailoring the pore structure of carbon nanofibers for achieving ultrahigh-energy-density supercapacitors using ionic liquids as electrolytes, J. Mater. Chem. A 4 (2016) 4763-4770.

[45] S. Chao, Y. Zhang, K. Wang, Z. Bai, L. Yang, Flower–like Ni and N codoped hierarchical porous carbon microspheres with enhanced performance for fuel cell

storage, Appl. Energ. 175 (2016) 421-428.

[46] Y. Yao, K.K. Fu, S. Zhu, J. Dai, Y. Wang, G. Pastel, Y. Chen, T. Li, C. Wang, T. Li, L. Hu, Carbon Welding by Ultrafast Joule Heating, Nano Lett. 16 (2016) 7282-7289.

[47] T. Lin, I.W. Chen, F. Liu, C. Yang, H. Bi, F. Xu, F. Huang, Nitrogen-doped mesoporous carbon of extraordinary capacitance for electrochemical energy storage, Science 350 (2015) 1508-1513.

[48] G. Bepete, Z.N. Tetana, S. Lindner, M.H. Rümmeli, Z. Chiguvare, N.J. Coville, The use of aliphatic alcohol chain length to control the nitrogen type and content in nitrogen doped carbon nanotubes, Carbon 52 (2013) 316-325.

[49] X. Tian, S. Zhu, J. Peng, Y. Zuo, G. Wang, X. Guo, N. Zhao, Y. Ma, L. Ma, Synthesis of micro- and meso-porous carbon derived from cellulose as an electrode material for supercapacitors, Electrochim. Acta 241 (2017) 170-178.

[50] C. Liu, Y. Tan, Y. Liu, K. Shen, B. Peng, X. Niu, F. Ran, Microporous carbon nanofibers prepared by combining electrospinning and phase separation methods for supercapacitor, Journal of Energy Chemistry 25 (2016) 587-593.

[51] W. Nan, Y. Zhao, Y. Ding, A.R. Shende, H. Fong, R.V. Shende, Mechanically flexible electrospun carbon nanofiber mats derived from biochar and polyacrylonitrile, Mater. Lett. 205 (2017) 206-210.

[52] A. Chen, K. Xia, L. Zhang, Y. Yu, Y. Li, H. Sun, Y. Wang, Y. Li, S. Li, Fabrication of Nitrogen-Doped Hollow Mesoporous Spherical Carbon Capsules for Supercapacitors, Langmuir. 32 (2016) 8934-8941.

[53] Shilpa, A. Sharma, Free standing hollow carbon nanofiber mats for supercapacitor electrodes, RSC Advances 6 (2016) 78528-78537.

[54] J. Yan, J.-H. Choi, Y.G. Jeong, Freestanding supercapacitor electrode applications of carbon nanofibers based on polyacrylonitrile and polyhedral oligomeric silsesquioxane, Mater. Design. 139 (2018) 72-80.

[55] M.A.A. Mohd Abdah, N.A. Zubair, N.H.N. Azman, Y. Sulaiman, Fabrication of PEDOT coated PVA-GO nanofiber for supercapacitor, Mater. Chem. Phys. 192 (2017) 161-169.

[56] Z. Li, L. Yang, H. Cao, Y. Chang, K. Tang, Z. Cao, J. Chang, Y. Cao, W. Wang, M. Gao, C. Liu, D. Liu, H. Zhao, Y. Zhang, M. Li, Carbon materials derived from chitosan/cellulose cryogel-supported zeolite imidazole frameworks for potential supercapacitor application, Carbohyd. Polym. 175 (2017) 223-230.

Crosslinked carbon nanofiber films with hierarchical pores as flexible electrodes for high performance supercapacitors

Jianping Ding [a, b], Hong-ping Zhang [a, *], Xiaodong Li [b, *], Youhong Tang [c], Guangcheng Yang [b]

[a] Engineering Research Center of Biomass Materials, Ministry of Education, School of Materials Science and Engineering, Southwest University of Science and Technology, Mianyang, Sichuan 621010, China

[b] Institute of Chemical Materials, China Academy of Engineering Physics, Mianyang, Sichuan 621900, China

[c] Centre for NanoScale Science and Technology, College of Science and Engineering, Flinders University, South Australia 5042, Australia

[*] Corresponding authors. Tel: +86-816-6089009, Fax: +86-816-6089009, E-mail: zhp1006@126.com (H. P. Zhang); Tel: +86-816-2544426, Fax: +86-816-2544426, E-mail: lixdong2013@caep.cn (X. D. Li)

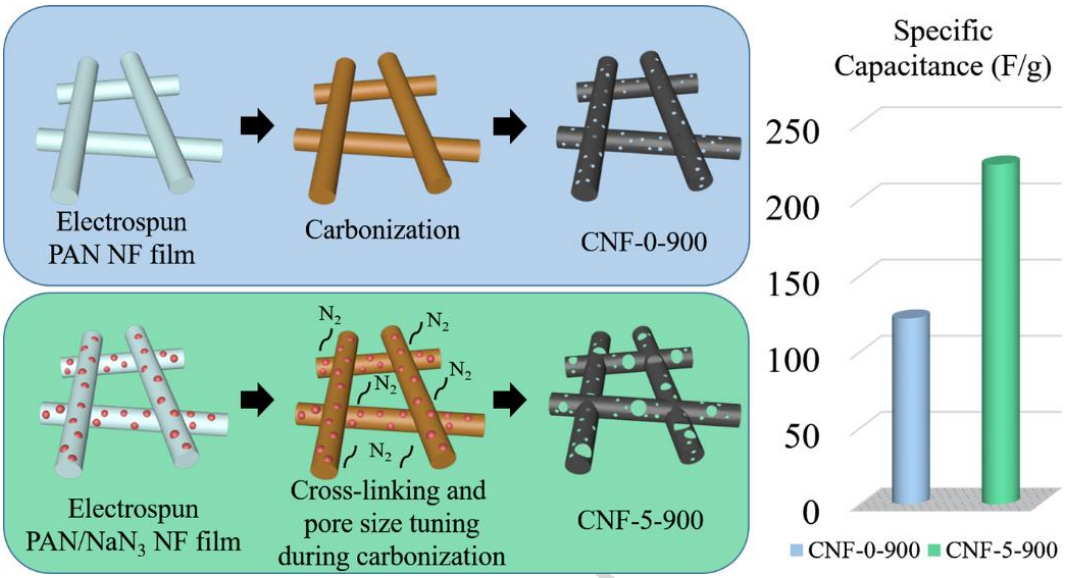

Graphical abstract

Crosslinked carbon nanofiber films with hierarchical pores as flexible electrodes for high performance supercapacitors

Jianping Ding, Hong-ping Zhang, Xiaodong Li, Youhong Tang, Guangcheng Yang

Highlights

- Flexible CNFs films with hierarchical micro-meso-macro-porous structure are prepared.
- Pore structure of the CNFs can be tuned by gas liberation of NaN_3.
- Exothermal decomposition of NaN_3 leads to the cross-linked structure in CNFs films.
- CNF based supercapacitors show high specific capacitance and excellent rate ability.